

Chapter 8

Reservoir Engineering

As we have seen, decoherence in our system is undesirable, inasmuch as it limits our ability to perform quantum state engineering and quantum logic operations. In order to do large-scale quantum computation, we must understand the sources of decoherence and be able to reduce them, at least to the levels where fault-tolerant error correction becomes possible. However, the general phenomenon of decoherence (nebulous though this title may be) is of interest in itself. The entanglement of a quantum system with inaccessible and/or uncontrollable degrees of freedom of the environment has attracted much attention [15] as a possible way of explaining how the microscopic world described by quantum mechanics transforms to the macroscopic world which we appear to inhabit. In particular, in the macroscopic world there seems to be no evidence of the superposition and entanglement behaviours which lie at the very heart of quantum mechanics.

It is therefore desirable to be able to study decoherence in a well-controlled manner. Since our trapped-ion system exhibits controllable coherent behaviour of two coupled basic quantum systems, it offers a “test bed” for examining various aspects of system-reservoir interactions leading to decoherence. Recently, we have been able to study the interaction of the ion motion with various electric-field configurations which produce theoretically well-understood reservoir interactions. Since the harmonic oscillator is often the “system of choice” for theorists (due to its simple nature), it is partic-

ularly easy to draw the correspondence between experiment and theory in this system. Furthermore, the control we have over the harmonic oscillator coupling to other degrees of freedom (see Ch. 3) allows us to explore a large region of the “parameter space” described by different theories.

In particular, we have been able to realize so-called “amplitude, “phase,” and “zero temperature” reservoir interactions with the ion’s motion. In this chapter, I will briefly overview some of the theoretical background on reservoir interactions and decoherence theory and then discuss the experiments which realized the particular reservoir interactions listed above.

8.1 Reservoir Interactions and Decoherence

Schrödinger’s equation is the fundamental equation of quantum mechanics: it describes the time evolution of a closed quantum mechanical system. In general, however, quantum systems are *not* closed: all systems which we can ever encounter in the real world are coupled to other parts of that real world, however weakly.¹ In essence, this coupling provides a route for (partial) information about the quantum state of the system under consideration to “leak” into the “rest of the world.” If we perform measurements on only the subsystem under consideration, this loss of information results in a loss of coherence.

One way to model the effects of this leak of information to uncontrollable and inaccessible degrees of freedom is through a “master equation” for the density matrix of the quantum system of interest. We may follow the approach of Carmichael [185] and others [124, 186] in order to derive a general master equation. Consider a quantum system S which interacts with its environment. I will refer to the environment as R , which stands for “reservoir:” this highlights the idea that the environment has very

¹ One may, perhaps, consider the *entire universe* as a closed quantum system. However, no matter how stimulating this may be, we will certainly never have experimental access to the *entire universe*!

many degrees of freedom and that, though the environment may have a large effect on the system S , the system will have very little effect on the overall state of the environment.

The overall Hamiltonian for the two, coupled quantum systems (S and R), is

$$\hat{H} = \hat{H}_S + \hat{H}_R + \hat{H}_{SR}. \quad (8.1)$$

Here \hat{H}_S and \hat{H}_R are the free Hamiltonians of the system and reservoir, respectively (in the absence of any coupling between the two). \hat{H}_{SR} represents the coupling between S and R . In general, \hat{H}_{SR} will have the form:

$$\hat{H}_{SR} = \hbar \sum_i \hat{s}_i \hat{\Gamma}_i, \quad (8.2)$$

where the \hat{s}_i are operators which act only in the Hilbert space of the system and the $\hat{\Gamma}_i$ are operators which act only in the Hilbert space of the reservoir (environment). The sum is over all the different parts (modes) of the environment: typically this sum is taken to be infinite. As a concrete example, in the case of the damping of a harmonic oscillator system's amplitude into a reservoir of harmonic oscillators, we will may take $\hat{s}_1 = \hat{a}, \hat{s}_2 = \hat{a}^\dagger, \hat{\Gamma}_1 = \sum_i \kappa_i^* \hat{b}_i^\dagger$, and $\hat{\Gamma}_2 = \sum_i \kappa_i \hat{b}_i$, where $\hat{b}_i, \hat{b}_i^\dagger$ are the lowering and raising operator of the reservoir mode harmonic oscillators. We will return to this model later.

Let the complete density matrix for $S \oplus R$ be $\hat{\chi}(t)$, and

$$\hat{\rho}(t) = \text{tr}_R[\hat{\chi}(t)] \quad (8.3)$$

be the reduced density operator of the system alone. The goal is to determine an equation of motion for $\hat{\rho}(t)$, since this is the state which we actually wish to, and are able to, measure.² The result of a measurement of a system operator \hat{O} , which is given by $\langle \hat{O} \rangle = \text{tr}_{S \oplus R}[\hat{O}\hat{\chi}(t)] = \text{tr}_S\{\hat{O}\text{tr}_R[\hat{\chi}(t)]\} = \text{tr}_S[\hat{O}\hat{\rho}(t)]$, depends only on $\hat{\rho}(t)$ and not on the complete density matrix $\hat{\chi}(t)$.

² Even if we wished to measure the state of the environment R , we would not be able to completely determine the complete state of the rest of the universe! Thus, we cut our losses and concentrate on what we *can* measure.

In an interaction picture defined by $\hat{U}(t) = \exp[i(\hat{H}_S + \hat{H}_R)/\hbar]$, the equation of motion for the complete (interaction- picture) density matrix is given by:

$$\dot{\hat{\chi}}' = \frac{1}{i\hbar}[\hat{H}'_{SR}(t), \hat{\chi}'], \quad (8.4)$$

where \hat{H}'_{SR} is the interaction-picture coupling Hamiltonian.³ Eq. (8.4) may be perturbatively solved [185, 124]. First, we may formally integrate the equation and plugging the result back into Eq. 8.4:

$$\hat{\chi}'(t) = \hat{\chi}'(0) + \frac{1}{i\hbar} \int_0^t [\hat{H}'_{SR}(\tilde{t}), \hat{\chi}'(\tilde{t})] d\tilde{t} \quad (8.5)$$

$$\Rightarrow \hat{\chi}'(t) = \frac{1}{i\hbar} [\hat{H}'_{SR}(t), \hat{\chi}'(0)] - \frac{1}{\hbar^2} \int_0^t [\hat{H}'_{SR}(t), [\hat{H}'_{SR}(\tilde{t}), \hat{\chi}'(\tilde{t})]] d\tilde{t}. \quad (8.6)$$

By tracing over this equation, we will obtain the reduced density matrix for the system alone. Assume that, at time $t = 0$ (before the system-reservoir coupling is turned on), the system and reservoir are uncorrelated: $\hat{\chi}(0) = \hat{\rho}(0)\hat{R}_0$, where \hat{R}_0 is the initial reservoir density matrix. If we assume that $\text{tr}_R\{\hat{H}'_{SR}(t)\hat{R}_0\} = 0$, then the first term in Eq. (8.6) drops out in tracing over the reservoir. This is the case if reservoir operators $\hat{\Gamma}_i$ have expectation values of zero in the state R_0 : we may always make this so by including the term $\text{tr}_R\{\hat{H}_{SR}\hat{R}_0\}$ in the system Hamiltonian. Thus, the trace over the reservoir modes (with the above assumptions about the initial conditions), yields:

$$\dot{\hat{\rho}}' = -\frac{1}{\hbar^2} \int_0^t \text{tr}_R \left\{ [\hat{H}'_{SR}(t), [\hat{H}'_{SR}(\tilde{t}), \hat{\chi}'(\tilde{t})]] \right\}. \quad (8.7)$$

This equation is still exact: we have made no approximations in arriving at it. However, in general it exhibits an exceedingly complicated time dependence. Indeed, although the system and reservoir are assumed to be uncorrelated initially, (i.e. the $t = 0$ density matrix factorizes) the interaction \hat{H}_{SR} causes them to become correlated at later times. This makes the problem very difficult to solve exactly. However, Eq. (8.7) is in a form which makes an iterative, perturbative solution relatively straightforward.

³ As in Ch. 3, I will use a prime to denote interaction-picture operators

If we assume that the coupling between the system and the reservoir is very weak, then we may make a perturbative expansion of the complete density matrix in the coupling \hat{H}_{SR} :

$$\begin{aligned}\hat{\chi}'(t) &= \hat{\rho}'(t)\hat{R}'(t) + \mathcal{O}(\hat{H}_{SR}) \\ &= \hat{\rho}'(t)\hat{R}_0 + \mathcal{O}(\hat{H}_{SR}).\end{aligned}\tag{8.8}$$

In writing the second line in Eq. (8.8), I have replaced $\hat{R}'(t)$ with \hat{R}_0 , the initial reservoir density matrix. The reasoning behind this is that R is so large that the coupling to S should have negligible effect on R . Another way of stating this is that the back-action on R of the coupling is negligible.

Now we may make a simplifying assumption: the “Born approximation” [2, 124]. This involves dropping the higher order terms in the expansion of $\hat{\chi}'(t)$ and substituting this approximation into Eq. (8.7). This gives us that

$$\dot{\hat{\rho}}' = -\frac{1}{\hbar^2} \int_0^t \text{tr}_R \left\{ [\hat{H}'_{SR}(t), [\hat{H}'_{SR}(\tilde{t}), \hat{\rho}'(\tilde{t})\hat{R}_0]] d\tilde{t} \right\}.\tag{8.9}$$

The Born approximation simplifies the equation of motion for the system density matrix somewhat, but Eq. (8.9) is still a complicated equation. In particular, the integral involves the value of the density matrix at all times from 0 to t . Thus, the time evolution of $\hat{\rho}'$ exhibits “memory” of its state at all previous times, which makes solving for the evolution very difficult. However, for many systems, it is possible to make a second approximation, the “Markoff approximation,” and replace $\hat{\rho}'(\tilde{t})$ by $\hat{\rho}'(t)$ under the integral sign. This is possible because the integrand also contains terms with \hat{H}'_{SR} evaluated both at t and at \tilde{t} . Depending on the properties of the *reservoir*, the integrand may then be negligible except when $\tilde{t} = t$.

To be more specific, let us plug in the explicit form for $\hat{H}'_{SR}(t)$ from Eq. (8.2) (transformed into the interaction picture). Then, Eq. (8.9) becomes:

$$\dot{\hat{\rho}}' = - \sum_{\{i,j\}} \int_0^t \text{tr}_R \left\{ [\hat{s}'_i(t)\hat{\Gamma}'_i(t), [\hat{s}'_j(\tilde{t})\hat{\Gamma}'_j(\tilde{t}), \hat{\rho}'(\tilde{t})\hat{R}_0]] \right\} d\tilde{t}$$

$$\begin{aligned}
&= - \sum_{\{i,j\}} \int_0^t \left\{ [\hat{s}'_i(t) \hat{s}'_j(\tilde{t}) \hat{\rho}'(\tilde{t}) - \hat{s}'_j(\tilde{t}) \hat{\rho}'(\tilde{t}) \hat{s}'_i(t)] \langle \hat{\Gamma}'_i(t) \hat{\Gamma}'_j(\tilde{t}) \rangle_R \right. \\
&\quad \left. + [\hat{\rho}'(\tilde{t}) \hat{s}'_j(\tilde{t}) \hat{s}'_i(t) - \hat{s}'_i(t) \hat{\rho}'(\tilde{t}) \hat{s}'_j(\tilde{t})] \langle \hat{\Gamma}'_j(\tilde{t}) \hat{\Gamma}'_i(t) \rangle_R \right\} d\tilde{t}. \quad (8.10)
\end{aligned}$$

In this equation, I have written:

$$\begin{aligned}
\langle \hat{\Gamma}'_i(t) \hat{\Gamma}'_j(\tilde{t}) \rangle_R &= \text{tr}_R \{ R_0 \hat{\Gamma}'_i(t) \hat{\Gamma}'_j(\tilde{t}) \} \\
\langle \hat{\Gamma}'_j(\tilde{t}) \hat{\Gamma}'_i(t) \rangle_R &= \text{tr}_R \{ R_0 \hat{\Gamma}'_j(\tilde{t}) \hat{\Gamma}'_i(t) \}, \quad (8.11)
\end{aligned}$$

which are the correlation functions of the reservoir, and used the fact that the trace operation is invariant under cyclic permutations of its argument. For many reservoir systems, the high density of reservoir states causes these correlation functions decay very rapidly. If this happens on a time scale short compared to the time evolution of $\hat{\rho}'$, then we may replace the (non-zero) correlation functions in Eq. (8.11) by delta functions:

$$\begin{aligned}
\langle \hat{\Gamma}'_i(t) \hat{\Gamma}'_j(\tilde{t}) \rangle_R &\rightarrow c_{ij} \delta(t - \tilde{t}) \\
\langle \hat{\Gamma}'_j(\tilde{t}) \hat{\Gamma}'_i(t) \rangle_R &\rightarrow c_{ji} \delta(t - \tilde{t}) \quad (8.12)
\end{aligned}$$

(where the c_{ij} 's are constants of proportionality). Then Eq. (8.10) becomes:

$$\begin{aligned}
\dot{\hat{\rho}}' &= \sum_{\{i,j\}} \left\{ c_{ij} [\hat{s}'_i(t) \hat{s}'_j(t) \hat{\rho}'(t) - \hat{s}'_j(t) \hat{\rho}'(t) \hat{s}'_i(t)] \right. \\
&\quad \left. + c_{ji} [\hat{\rho}'(t) \hat{s}'_j(t) \hat{s}'_i(t) - \hat{s}'_i(t) \hat{\rho}'(t) \hat{s}'_j(t)] \right\}. \quad (8.13)
\end{aligned}$$

This is the general master equation in the Born-Markoff approximation. Particular cases are obtained by choosing particular \hat{s}_i 's and $\hat{\Gamma}_i$'s.

I shall go on, in the next few sections, to discuss particular realizations of the master equation in our experiment. However, first, a few general comments on the above derivation are in order. This first comment is that this derivation was *general*: it dealt with the system and the reservoir modes in an explicitly quantum mechanical and somewhat abstract manner. The coupling Hamiltonian \hat{H}_{SR} was written down

in a general (though linear) form in Eq. (8.2) without specifying the particular system operators \hat{s}_i or the reservoir operators $\hat{\Gamma}_i$, and this general form was propagated through the entire derivation leading up to Eq. (8.13). However, careful examination of the steps leading to this equation shows that the quantum properties of the reservoir operators were never actually used in achieving the final result! The only place where the quantum nature of the reservoir becomes apparent is in writing down the \mathcal{C} -number correlation functions in Eq. (8.11), which are specifically ordered pairs of the $\hat{\Gamma}_i$'s. In this case, the constants of proportionality, $c_{i,j}$, in Eq. (8.12) may depend on the particular reservoir operators which are coupled to the system. However, since Eq. (8.12) evaluates to a constant \mathcal{C} -number, this information only feeds into the master equation in a parametric sense.

In this sense, the master equation describes quantum and “classical” reservoirs equally well! In essence, this comes about because of the approximations made in deriving the master equation: in particular, tracing over the reservoir states and making the Born and Markoff approximations. In making the Born approximation, we essentially ignore higher-order correlations in the reservoir, and in taking the trace over the reservoir state, we are reducing any functional dependence of the system reduced density matrix on the reservoir to a c -number. The Markoff approximation reduces the \mathcal{C} -number's functional form to a constant value. Because of these assumptions, the functional form of the master equation always remains the same: the most that a “non-classical” reservoir (e.g. a squeezed reservoir [124]) can “do” is to force the solutions of the equation into a region of parameter space that could never be explored by a system coupled to a classical reservoir.

8.1.1 Beyond the Master Equation

The idea of considering our quantum system as coupled to uncontrollable and inaccessible degrees of freedom of the “rest of the universe” marked the beginning of the

path which led to the master equation (in the Born-Markoff approximation). However, this idea has more general applications than just as a derivation of the master equation. Since these applications seem to be of some current interest, I will briefly touch on two of them.

Again, the idea is that the complete time evolution of the system plus reservoir is unitary, and governed by Schrödinger's equation. However, since we do not have information about the reservoir, we must (according to the usual prescription of quantum mechanics) trace over this part of the composite system, which leads to (apparently) non-unitary time evolution of the system considered by itself. Thus, an initial density matrix $\hat{\rho}(t=0)$ with $\text{tr}_S\{\hat{\rho}^2\} = 1$ evolves into a density matrix with $\text{tr}_S\{\hat{\rho}^2\} < 1$. However, we may still describe the system by a density matrix. Thus, although the time evolution is not described by a *unitary* operator, it is still described by a linear mapping, which maps linear operators to linear operators [43]. Such a linear mapping is referred to as a "superoperator." In particular [43, 187], we may express a superoperator \mathcal{M} as $\mathcal{M}(\hat{\rho}) = \sum_k \hat{M}_k \hat{\rho} \hat{M}_k^\dagger$, where the operators \hat{M}_k satisfy $\sum_k \hat{M}_k^\dagger \hat{M}_k = \mathbf{1}_s$.

In general, the evolution produced by this superoperator does not admit a description in terms of a differential equation. Such a description is only possible if the time evolution is *local* in time: i.e. Markovian. In this case, the reservoir (environment) does not retain a memory of the correlations between itself and the system, and so this information cannot "leak" back into the system. In this case, the dynamics of the system alone can be described by the master equation which we derived above.

In keeping with the operator/superoperator point of view, one often introduces a linear operator called the "Lindbladian." Given the Schrödinger equation,

$$\dot{\hat{\rho}} = -i/\hbar [\hat{H}, \hat{\rho}], \quad (8.14)$$

we may formally solve to obtain

$$\hat{\rho}(t) = e^{-i\hat{H}t/\hbar} \hat{\rho}(0) e^{i\hat{H}t/\hbar}. \quad (8.15)$$

We say that the Hamiltonian operator \hat{H} *generates* the time evolution. In the same way, for the non-unitary time evolution of a system in contact with a reservoir, one writes:

$$\dot{\hat{\rho}} = \mathcal{L}[\hat{\rho}] \quad (8.16)$$

$$\hat{\rho}(t) = e^{\mathcal{L}t}[\hat{\rho}] \quad (8.17)$$

and says that the linear operator \mathcal{L} , called the “Lindbladian,” generates the superoperator $\exp(\mathcal{L}t)$ which produces the time evolution. One then re-expresses the master equation, Eq. (8.13), as:

$$\begin{aligned} \dot{\hat{\rho}}' &= \mathcal{L}[\hat{\rho}'] \\ &= - \sum_{\{i,j\}} \left\{ c_{ij} [\hat{s}'_i(t) \hat{s}'_j(t) \hat{\rho}'(t) - \hat{s}'_j(t) \hat{\rho}'(t) \hat{s}'_i(t)] \right. \\ &\quad \left. + c_{ji} [\hat{\rho}'(t) \hat{s}'_j(t) \hat{s}'_i(t) - \hat{s}'_i(t) \hat{\rho}'(t) \hat{s}'_j(t)] \right\}. \end{aligned} \quad (8.18)$$

In this context, the operators \hat{s}'_i are often referred to as “Lindblad operators.”

This more general context allows for treatment of arbitrary system-environment interactions. Indeed, in all cases, the time evolution is described by a “master equation” (non-local in time!) similar in form to Eq. (8.10) [188]. Analysis of this equation shows that, in general, system-reservoir interactions are characterized by “pointer bases” of the system’s Hilbert space. A pointer basis state is invariant under the effects of the system-reservoir coupling Hamiltonian [15, 188, 189]. (We shall see some examples of pointer bases in the next few sections). Besides providing a convenient basis for analyzing the system dynamics, the general existence of a pointer basis regardless of the particular details of the system-environment interaction may help to resolve the apparent conflict between a quantum description of the world and our everyday, macroscopic experiences.

This conflict is illustrated by the example of “Schrödinger’s cat” (see Sec. 6.2.1). Although quantum mechanics generically allows for the existence of superpositions, we never see evidence for them on the macroscopic level. However, a general analysis of system-reservoir interactions [15, 188, 189, 190, 191, 192] indicates that the pointer

basis, which is often determined by the system operators appearing in the coupling Hamiltonian [188], forms a “preferred basis.” When the density matrix is expressed in this basis, one finds (as we shall, below) that the off-diagonal terms of the density matrix vanish as an exponential in the square of the “size” of the superposition (e.g. the square of $|m - n|$, where the density matrix elements are $\rho_{m,n}$). Since these off-diagonal terms are responsible for the interference effects which are the hallmark of superpositions [8], we never see macroscopic evidence of superpositions. Very often, the pointer states are position eigenstates, which may explain why position is a “good” classical observable. However, in some cases, energy eigenstates form the pointer basis [188]. This approach to the microscopic/macroscopic boundary is one of many, and many of its details are still being worked out. Nonetheless, it does seem to offer an attractive solution to the lack of interference effects on the macroscopic level.

In any event, the master equation, Eq. (8.13), allows us to make quantitative predictions for the behaviour of the density matrix elements for various forms of system-reservoir coupling. I will now examine some of these cases.

8.2 Phase Reservoir

A relatively simple example of the master equation occurs for the case of a harmonic oscillator of frequency ω_z (system) coupled to an infinite number of other harmonic oscillators (environment/reservoir) with a “phase damping” coupling [193]⁴ :

$$\begin{aligned}\hat{H}_{SR} &= \sum_k \hbar(\kappa_k^* \hat{b}_k^\dagger + \kappa_k \hat{b}_k) \hat{a}^\dagger \hat{a} \\ &= \hbar(\Gamma^\dagger + \Gamma) \hat{a}^\dagger \hat{a},\end{aligned}\tag{8.19}$$

Here, the $\hat{b}_k, \hat{b}_k^\dagger$ are the lowering and raising operators for the k^{th} reservoir mode and $\hat{\Gamma}$ is defined implicitly in the apparent manner. Making the connection with the derivation in Sec. 8.1.1, we identify $\hat{s}_1 = \hat{s}_2 = \hat{a}^\dagger \hat{a}$, $\hat{\Gamma}_1 = \Gamma^\dagger = \sum_k \kappa_k^* \hat{\Gamma}^\dagger$, and $\hat{\Gamma}_2 = \Gamma = \sum_k \kappa_k \hat{\Gamma}$.

⁴ Other authors (such as Ref. [185]) use a different system-reservoir coupling: $\hat{H}_{SR} = \sum_k \hbar \kappa_k \hat{b}_k^\dagger \hat{b}_k \hat{a}^\dagger \hat{a}$. This leads to the same master equation.

The reservoir is usually assumed to be in a thermal distribution at temperature T , so that

$$\hat{R}_0 = \prod_k \left(1 - e^{-\hbar\omega_k/k_B T}\right) e^{-\hbar\omega_k \hat{b}_k^\dagger \hat{b}_k / k_B T}. \quad (8.20)$$

This leads to the reservoir correlation functions:

$$\langle \hat{\Gamma}^{\dagger'}(t) \hat{\Gamma}^{\dagger'}(\tilde{t}) \rangle_R = 0 \quad (8.21)$$

$$\langle \hat{\Gamma}^{\dagger'}(t) \hat{\Gamma}'(\tilde{t}) \rangle_R = \sum_k |\kappa_k|^2 \overline{N}(\omega_k, T) e^{i\omega_k(t-\tilde{t})} \quad (8.22)$$

$$\langle \hat{\Gamma}'(t) \hat{\Gamma}^{\dagger'}(\tilde{t}) \rangle_R = \sum_k |\kappa_k|^2 [\overline{N}(\omega_k, T) + 1] e^{i\omega_k(t-\tilde{t})} \quad (8.23)$$

$$\langle \hat{\Gamma}'(t) \hat{\Gamma}'(\tilde{t}) \rangle_R = 0, \quad (8.24)$$

where

$$\overline{N} = \frac{e^{-\hbar\omega_z/k_B T}}{1 - e^{-\hbar\omega_z/k_B T}} \quad (8.25)$$

is the average occupation number of the reservoir mode k .

If we plug in from Eqs. (8.25) for the reservoir correlation functions and replace the sum over the reservoir modes by an integral, with density of states $g(\omega)$, then Eq. (8.10) becomes:

$$\begin{aligned} \dot{\rho}' &= - \int_{\omega=0}^{\infty} \int_{\tau=0}^t \\ &\left\{ 2[\hat{n}^2 \hat{\rho}'(\tilde{t}-\tau) - 2\hat{n} \hat{\rho}'(\tilde{t}-\tau) \hat{n} + \hat{\rho}'(\tilde{t}-\tau) \hat{n}^2] g(\omega) |\kappa(\omega)|^2 \overline{N}(\omega, T) e^{i\omega\tau} \right. \\ &\left. [\hat{n}^2 \hat{\rho}'(\tilde{t}-\tau) - 2\hat{n} \hat{\rho}'(\tilde{t}-\tau) \hat{n} + \hat{\rho}'(\tilde{t}-\tau) \hat{n}^2] g(\omega) |\kappa(\omega)|^2 e^{i\omega\tau} \right\} d\tilde{t} d\omega. \quad (8.26) \end{aligned}$$

In Eq. (8.26), $\tau \doteq t - \tilde{t}$. However, the time scales of interest to us are much longer than the time scales over which the time integrand has appreciable values. To see this, assume that $\kappa(\omega)$ and $g(\omega)$ are constant in Eq. (8.26). Then the integrals are just the Fourier transform of the function $\overline{N}(\omega, T)$; at room temperature, the relevant reservoir time scales are on the order of 10^{-14} s, much faster than the microsecond time scales of interest in our experiments. With this in mind, we can replace $t - \tau$ with t in Eq. (8.26) (the Markoff approximation). This is sometimes referred to as ‘‘coarse graining.’’

When we make this replacement, we obtain the master equation for the density matrix:

$$\begin{aligned}\dot{\hat{\rho}}'(t) &= -\mathcal{A}[\hat{n}^2\hat{\rho}'(t) - 2\hat{n}\hat{\rho}'(t)\hat{n} + \hat{\rho}'(t)\hat{n}^2] \\ &+ -2\mathcal{B}[\hat{n}^2\hat{\rho}'(t) - 2\hat{n}\hat{\rho}'(t)\hat{n} + \hat{\rho}'(t)\hat{n}^2],\end{aligned}\quad (8.27)$$

where

$$\mathcal{A} = \int_{\omega=0}^{\infty} \int_{\tau=0}^t g(\omega)|\kappa(\omega)|^2 e^{i\omega\tau} d\tilde{t} d\omega \quad (8.28)$$

$$\mathcal{B} = \int_{\omega=0}^{\infty} \int_{\tau=0}^t g(\omega)|\kappa(\omega)|^2 e^{i\omega\tau} \overline{N}(\omega, T) d\tilde{t} d\omega \quad (8.29)$$

$$(8.30)$$

Again recognizing the separation of time scales between the reservoir correlation times (significant values of τ) and the system evolution (significant values of t), we can extend the time integral to $+\infty$ in Eqs. (8.30). When we do this, the integrals can be expressed as Dirac delta-functions in frequency. We also end up with terms containing the Cauchy principal values of the integrands, but these correspond to small shifts of the harmonic oscillator frequency [185] (analogous to the Lamb shift), and can be absorbed into this frequency. Tying all this together, we finally obtain the master equation for a harmonic oscillator coupled to a reservoir with a phase-damping coupling:

$$\dot{\hat{\rho}}' = \kappa \left(\hat{a}^\dagger \hat{a} \hat{\rho}' \hat{a}^\dagger \hat{a} - \frac{1}{2} (\hat{a}^\dagger \hat{a})^2 \hat{\rho}' - \frac{1}{2} \hat{\rho}' (\hat{a}^\dagger \hat{a})^2 \right), \quad (8.31)$$

where $\kappa = 6\pi g(0)|\kappa(0)|^2$ is the effective coupling strength.

This master equation is straightforward to solve, if we express the density matrix in the Fock state basis: $\hat{\rho}' = \sum_{n,m} \rho'_{nm} |n\rangle\langle m|$. In this case, using the properties of the number operator $\hat{n} = \hat{a}^\dagger \hat{a}$, we have that

$$\begin{aligned}\dot{\rho}'_{nm} &= \kappa \left(nm - \frac{1}{2}n^2 - \frac{1}{2}m^2 \right) \rho'_{nm} \\ &= -\frac{1}{2}\kappa(n-m)^2 \rho'_{nm}.\end{aligned}\quad (8.32)$$

Thus, the density matrix is given by:

$$\rho'_{nm}(t) = \rho_{nm}(0)e^{-\frac{1}{2}\kappa(n-m)^2t}. \quad (8.33)$$

So, for example, if we make states such as $|\psi_p\rangle = (|n\rangle + |m\rangle)/\sqrt{2}$, then the coherences should decay like $e^{-\kappa(n-m)^2t/2}$. Note that the diagonal elements suffer no decay at all.

For this reservoir coupling, then, the Fock states play the role of a pointer basis⁵. When the density matrix is expressed in this basis, the diagonal elements do not decay, but the off-diagonal elements do. Furthermore, superpositions of widely different Fock states (i.e. “mesoscopic” superpositions) suffer extremely rapid decay of the coherences. Thus, “mesoscopic” superposition states quickly decay to mixtures.

In order to observe the effects of the coupling to the reservoir, we prepared “cat-like” states of the form $|s\rangle(|n\rangle + |m\rangle)/\sqrt{2}$ (where $|s\rangle \in \{\downarrow, \uparrow\}$) as discussed in Sec. 6.1.2. For example, the state $|\downarrow\rangle(|0\rangle + |2\rangle)/\sqrt{2}$ was prepared by first performing a $\pi/2$ -pulse on the blue sideband, then performing a π -pulse on the red sideband. After allowing the state to interact with a phase reservoir (see below), we then reversed the state preparation. Thus the experiment consisted of preparing a superposition state, allowing the state to interact with the environment for some period of time and then reversing the superposition. In this respect, it resembled a Ramsey experiment (see Sec. 3.4). Indeed, by sweeping the frequency of the $\pi/2$ - pulses, we could sweep out Ramsey fringes. Decoherence which occurred in between the two “Ramsey zones” (superposition creation and reversal) reduced the contrast of the Ramsey fringes.

At each frequency, we repeated the experiment ≈ 100 times and measured the average cycling-transition photon counts, to build up a Ramsey curve. Since the Ramsey experiment connected the motional states $|n\rangle$ and $|m\rangle$, it was sensitive to the off-diagonal

⁵ In general, the “ideal” pointer states are eigenstates of system operators \hat{O}_S , where $[\hat{H}_{SR}, \hat{O}_S] = 0$. In this case, the pointer basis is exactly the Fock state basis. For the case of amplitude coupling, which we shall treat below, the coherent states are an approximate, but not exact, pointer basis.

motional density matrix elements ρ_{nm} . From the treatment above, we would then expect the contrast of the Ramsey fringes to scale as $\exp[-\kappa(n-m)^2 t_{res}/2]$.

The effect of a phase reservoir is to cause a random change in the ion's motional phase without affecting the ion's eigenstate distribution. One way to realize such an interaction is to change the trap frequency in a random fashion: this causes the time evolution operator $\hat{U}(t) = e^{i\hat{n}\omega_z t} \rightarrow e^{i\hat{n}(\omega_z + \delta\omega)t/\hbar}$. If the trap frequency is changed for a time t_{res} , then the resultant phase shift in the ion's wave function is given by:

$$\delta\phi = \int_0^{t_{res}} \delta\omega dt. \quad (8.34)$$

We changed the trap frequency by applying a noisy voltage to one of the middle segments of the linear trap's electrode structure, for a time $t_{res} = 20 \mu\text{s}$ in between the Ramsey zones. This produced a field gradient at the ion which, according to Eq. (2.54), altered the trap frequency. We ensured that the trap frequency change was adiabatic by filtering the noise: the noise source was a 10 MHz white noise source, which was then filtered to produce a spectrum which was flat from $\approx 1 - 100$ kHz, then rolled off at 18 dB/octave⁶. This filtering was necessary to reduce the frequency components at ω_z , which would have excited the ion's motion (see Sec. 6.1.3). From studying the axial trap frequency as a function of static voltage applied to the trap electrodes, we knew that the shift in the trap frequency was 90 kHz/V, so that the expected phase shift for an applied voltage shift δV was:

$$\delta\phi = (90 \text{ kHz/V}) \int_0^{20 \mu\text{s}} \delta V dt. \quad (8.35)$$

Although one may use the master equation approach to deal with this situation, it is also possible to use a semi-classical model to predict the behaviour of the ion's motion in this situation. Since the trap change was adiabatic, we may view the trap strength as essentially constant in each shot of the experiment, but random from shot

⁶ Additional filtering was provided by the filter network on the trap electrode structure (see Sec. 2.4.2).

to shot. The phase shift due to the differing trap strength resulted in an additional phase $e^{i\delta\phi n}$ on the Fock state $|n\rangle$. Thus, the effect of the changed trap strength was to produce a phase shift $e^{i\delta\phi(n-m)}$ in the cat-like state $|s\rangle(|n\rangle + |m\rangle)/\sqrt{2}$, which varied in a random fashion from shot to shot of the experiment. This phase mapped onto the Ramsey fringes, which, when averaged over the random voltage change, caused a loss of Ramsey fringe contrast. Applying this averaging procedure, one finds that the Ramsey fringe contrast should degrade exponentially in $(n - m)^2$.

The exponential in the square of the Fock state difference is the same as predicted by the master equation approach. In this case, the behaviour of the reservoir is classical, and so there is a semi-classical treatment of the interaction which exactly mimics the behaviour of the master equation (and vice-versa!). This is an example of the generality of the master equation approach, as discussed following Eq. (8.13). One might object that each individual experiment was describable by a state vector (i.e. unitary time evolution) and, therefore, that the situation is not one described by the master equation. However, the experiments as a whole represented an *ensemble* of identically prepared quantum systems, which correspond to a density matrix. In fact, any (non pure-state) density matrix admits any number of interpretations as an ensemble preparation [43, 187]. The behaviour of the ensemble as a whole is irrespective of the particular details of how the ensemble was realized. So the master equation is also an appropriate description of the experiment.

Of course, in principle, we could have measured the (classical) electric field gradient in each shot of the experiment, and applied a calculated phase shift to that data point, to reconstruct the Ramsey fringes with 100% contrast even in the presence of the noisy electric field. But, in fact, we did not do this and, as pointed out by Preskill [43] (for example), the situation where we have a quantum system considered by itself and one where we also have information about how that system has interacted with other

systems are fundamentally different, and have a different mathematical description. (This is illustrated by so-called “quantum eraser” experiments [194, 195, 196]).

We repeated the experiment while varying the rms voltage noise \mathcal{V} , measuring the contrast of the Ramsey fringes at each point. Fig. 8.1 shows the Ramsey fringe contrast in our experiment as a function of the applied mean squared voltage, scaled by $(n - m)^2$. The data are also rescaled to give unity contrast at $\mathcal{V} = 0$, correcting for a small loss of contrast due to sources of technical noise and due to the background source of motional heating (see Secs. 5.5, 8.3.1). All the data points fall on the universal curve predicted by theory (master equation or ensemble average).

8.3 Amplitude Reservoir

Another particular form of the master equation comes about by considering a harmonic oscillator of frequency ω_z (system) coupled to an infinite number of other harmonic oscillators (environment/reservoir) in the so-called “amplitude reservoir” case. In this case, the coupling is given by

$$\begin{aligned}\hat{H}_{SR} &= \sum_k \hbar \kappa_k (\hat{a} \hat{b}_k^\dagger + \hat{a}^\dagger \hat{b}_k) \\ &= \hbar (\hat{a} \hat{\Gamma}^\dagger + \hat{a}^\dagger \hat{\Gamma}),\end{aligned}\tag{8.36}$$

where, again, the \hat{b}_k , \hat{b}_k^\dagger are the lowering and raising operators for the k^{th} reservoir mode and $\hat{\Gamma}$, $\hat{\Gamma}^\dagger$ are the sums of these operators over the reservoir modes. Making the connection with the derivation in Sec. 8.1.1, we identify $\hat{s}_1 = \hat{a}$, $\hat{s}_2 = \hat{a}^\dagger$, $\hat{\Gamma}_1 = \sum_k \kappa_k^* \hat{b}_k^\dagger$, and $\hat{\Gamma}_2 = \sum_k \kappa_k \hat{b}_k$.

The derivation of the master equation is very similar to the derivation for the phase-damping case (Sec. 8.2). The resulting master equation is:

$$\dot{\rho}' = \kappa(2\hat{a}\hat{\rho}'\hat{a}^\dagger - \hat{a}^\dagger\hat{a}\hat{\rho}' - \hat{\rho}'\hat{a}^\dagger\hat{a}) + 2\kappa\overline{N}(\hat{a}\hat{\rho}'\hat{a}^\dagger + \hat{a}^\dagger\hat{\rho}'\hat{a} - \hat{a}^\dagger\hat{a}\hat{\rho}' - \hat{\rho}'\hat{a}\hat{a}^\dagger).\tag{8.37}$$

The analysis of the dynamics induced by this master equation is tedious [191]. There are two significant results. One is that the approximate pointer states for this coupling

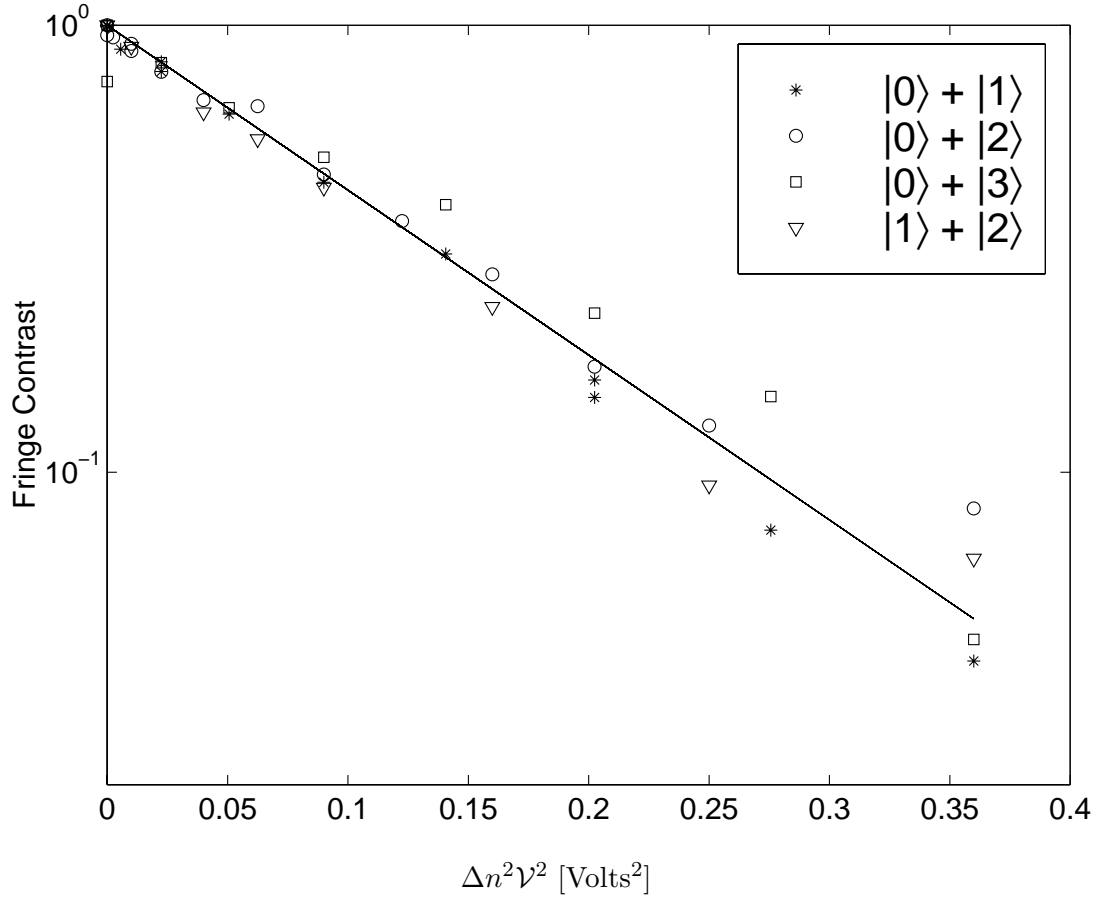


Figure 8.1: “Ramsey” fringe contrast as a function of coupling strength to phase reservoir. The x -axis is in terms of the square of the rms voltage \mathcal{V} applied to the middle electrode of the trap, scaled by the square of the “size” Δn of the superposition state, and the fringe contrast is normalized to unity at $\mathcal{V} = 0$. The solid line is a one-parameter (slope) fit to an exponential, constrained to be unity at $\mathcal{V} = 0$.

are the coherent states $|\alpha\rangle$ (see Sec. 6.1.3). The second is that, again, the off-diagonal density matrix elements decay much faster than elements on the diagonal.

In order to observe the effects of the coupling to the reservoir, we prepared “Schrödinger cat” states of the form $(|\downarrow, \alpha_\downarrow\rangle + |\uparrow, \alpha_\uparrow\rangle)/\sqrt{2}$, as discussed in Sec. 6.2.1. Again, the cat preparation and reversal procedure can be viewed as a Ramsey-type experiment — and again, decoherence which occurred in between the two Ramsey zones reduced the contrast of the Ramsey fringes.

In our case, we obtained Ramsey fringes by sweeping the frequency of the $\pi/2$ -pulses on the carrier transition (the first and the last pulses of the preparation/reversal pulse sequence). At each frequency, we repeated the experiment ≈ 100 times and measured the average intensity, to build up a Ramsey curve. A treatment following the work of Collett [191] shows that, in the high-temperature limit, we would expect Ramsey fringes of the form:

$$P_{\downarrow}(t_{res}) = \frac{1}{2} \left(1 - e^{-2|\Delta\alpha|^2(1+\overline{N}\kappa t_{res})} \cos(\delta) \right). \quad (8.38)$$

In Eq. (8.38), δ is the detuning of the carrier $\pi/2$ - pulses from resonance and $|\Delta\alpha|^2$ is the square of the separation between the two coherent states constituting the cat state.

The form of the coupling, Eq. (8.36), which contains a sum of the system operators \hat{a} and \hat{a}^{\dagger} , suggest that the effects of the reservoir may be realized by applying displacement operators to the ion. That is, indeed, the case: the reservoir may be realized by applying noisy electric fields to the ion, with a noise spectrum centred around the trap frequency ω_z . As long as the bandwidth of the noise is large enough⁷, this will be a realization of the amplitude reservoir. In the experiment, we applied the noisy field to the trap electrodes for $3 \mu\text{s}$ in between the cat creation and reversal steps. We repeated the experiment while varying the rms voltage noise \mathcal{V} and the separation $\Delta\alpha$ between the cat wave packets, measuring the contrast of the Ramsey fringes at each point.

As with the phase reservoir case, the experiment may be analyzed either using the master equation or a semi-classical average over the shot-to-shot variations in the electric field strength (or noise voltage, \mathcal{V}). In this latter point of view, we may view the electric field as producing a displacement $\hat{D}(\beta)$ which varied from shot to shot of the experiment. Since the electric field affected both $|\downarrow\rangle$ and $|\uparrow\rangle$ the same, both components of the cat state suffered the same displacement $\hat{D}(\beta)$. Thus, the state

⁷ In practice, if the bandwidth of the noise is large compared with t_{res} , then the bandwidth is effectively infinite

reversal still succeeded in undoing the cat creation with 100% fidelity! However, the additional displacement resulted in an additional phase between $|\downarrow\rangle$ and $|\uparrow\rangle$, so that the state after the reversal was [50]:

$$|\psi\rangle' = \frac{1}{\sqrt{2}} \left(|\downarrow\rangle + e^{2i\text{Im}(\beta)\Delta\alpha^*} |\uparrow\rangle \right). \quad (8.39)$$

Thus, there was a random phase in the Ramsey fringes which was random from shot to shot of the experiment. When averaged over the random variable β , this caused a loss of Ramsey fringe contrast, which should have had the form $e^{-\kappa\Delta\alpha^2\mathcal{V}^2}$ (where κ is a coupling constant between the applied voltage and the ion motion), as with the master-equation analysis.

Figure 8.2 shows the Ramsey fringe contrast in our experiment as a function of the applied mean squared voltage, scaled by $|\Delta\alpha|^2$. As with the phase noise data, the data are scaled to give unity contrast at $\mathcal{V} = 0$. All the data points fall on the universal curve predicted by theory (master equation or ensemble average).

8.3.1 Natural Amplitude Reservoir

As discussed in Sec. 5.5, an ambient heating source exists in the trap, whose exact nature is as-yet poorly understood. This source represents an ambient $T \neq 0$ reservoir, and should produce the same behaviour in cat states as the applied amplitude reservoir. Indeed, preliminary evidence of this was reported in Ref. [47]. In order to quantify this decoherence, we varied the time between creating the cat states and reversing them, while varying the size $\Delta\alpha$ of the cats. The Ramsey fringe visibility as a function of $\Delta\alpha^2 t_{res}$ is shown in Fig. 8.3. Again, the fringe visibility is exponential in $\Delta\alpha^2$: the visibility decays as $e^{-\gamma\Delta\alpha^2 t_{res}}$. The decay constant, obtained by fitting a straight line to the scaled data, is $\gamma = 6.7 \times 10^{-3}/\mu\text{s}$, which is consistent with the heating rates in the linear trap (see Sec. 5.5 or Ref. [45]).

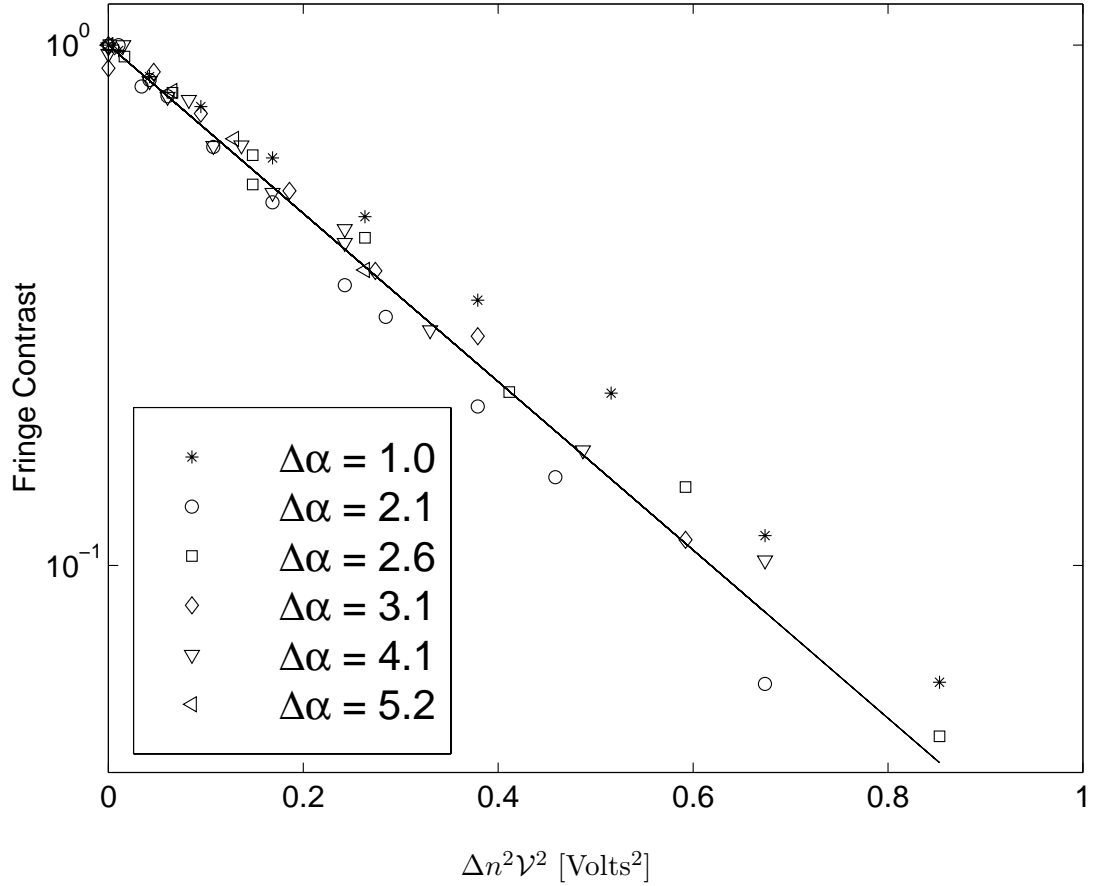


Figure 8.2: “Ramsey” fringe contrast as a function of coupling strength to an amplitude reservoir. The x -axis is in terms of the square of the rms voltage \mathcal{V} applied to the trap electrodes, scaled by $|\Delta\alpha|^2$ (the square of the “size” of the superposition state), and the fringe contrast is normalized to unity at $\mathcal{V} = 0$. The solid line is a one-parameter (slope) fit to an exponential, constrained to be unity at $\mathcal{V} = 0$.

8.4 Engineered $T=0$ Reservoir

The $T = 0$ limit of the thermal reservoir (amplitude coupling) is not straightforward to realize with noisy, classical electric fields (which may always be expressed as an equivalent Johnson noise in a resistor at finite temperature T [114]). However, we do have ready access to a $T = 0$ reservoir in the form of laser cooling (see Ch. 5). This connection was first pointed out by Poyatos, Cirac, and Zoller [197]. In this case, the coupling is between the laser beams (representing a $T = 0$ reservoir) and the ion

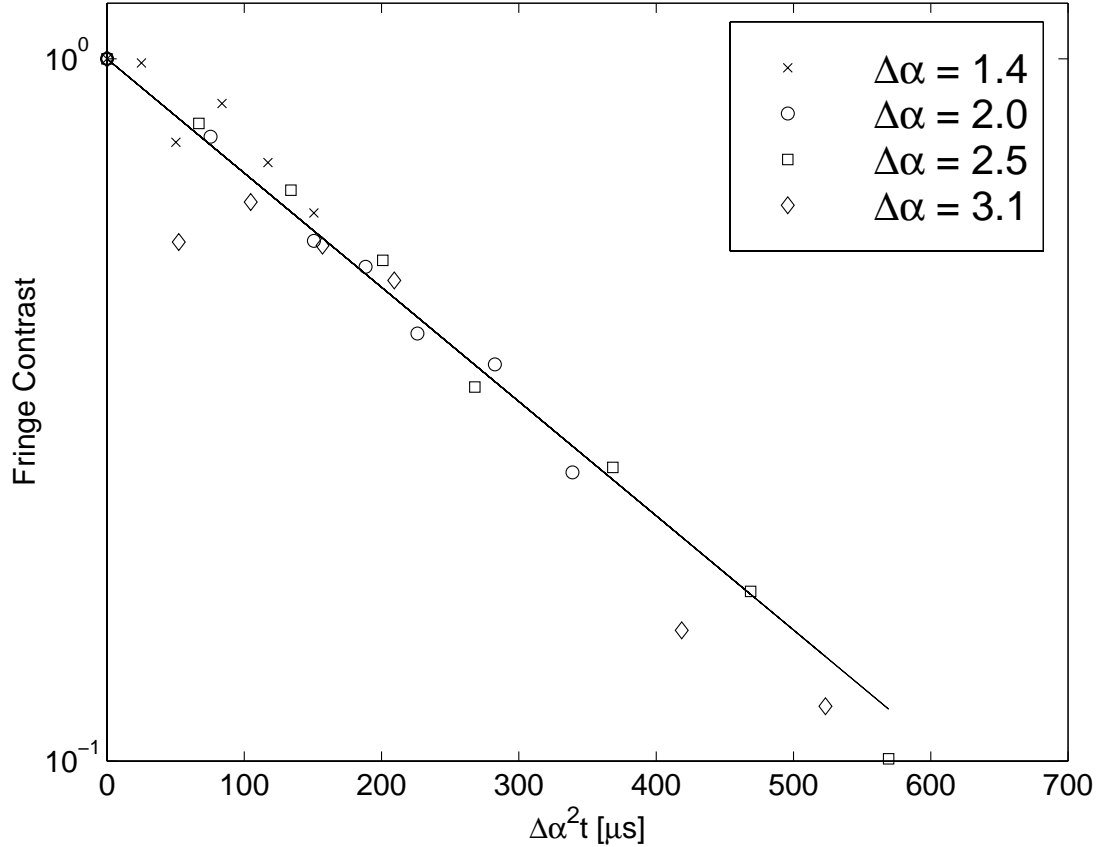


Figure 8.3: “Ramsey” fringe contrast as a function of interaction time with the “natural” amplitude reservoir due to the background heating rate in the trap. The x -axis is in terms of the interaction time t , scaled by $|\Delta\alpha|^2$ (the square of the “size” of the superposition state, and the fringe contrast is normalized to unity at $t = 0$). The solid line is a one-parameter (slope) fit to an exponential, constrained to be unity at $t = 0$.

motion [197]. The dissipation is due to the inherently random nature of the spontaneous emission during the recycling process. In interacting with the zero-temperature reservoir, the ion relaxes into a “dark state:” the state $|n = 0\rangle$, which is unaffected by the reservoir coupling. The complete reservoir interaction consists of a coherent part, which transfers the spin population from $|\downarrow\rangle$ to $|\uparrow\rangle$ while coherently reducing the phonon number, and an incoherent repumping from $|\uparrow\rangle$ to $|\downarrow\rangle$ (in this case, through the $2p^2P_{1/2}$ level⁸).

⁸ These experiments were performed with the the repumper laser resonant with transitions to the $2p^2P_{1/2}$ level, as discussed in Sec. 4.1.3.

The decoherence of cat states into an ambient, $T \approx 0$ reservoir has been observed before, in a Cavity-QED system [198]. However, in our case, we had the ability to “engineer” the characteristics of the reservoir interaction. By changing the relative intensities of the red sideband Raman beams and the repumping beam (the red doppler), we could change the ratio of the coherent to the incoherent pump rates. This was possible because (in contrast to the original proposal) our system actually consisted of three electronic levels: $|\downarrow\rangle$, $|\uparrow\rangle$, and the $2p \ ^2P_{1/2}$. The decay rate γ from the $2p \ ^2P_{1/2}$ level was much larger (≈ 20 MHz) than the Rabi frequency of the $|\uparrow\rangle \rightarrow 2p \ ^2P_{1/2}$ transition ($\ll 1$ MHz) so that the decay from this level could be considered instantaneous. The “bottleneck” in the population transfer was thus the Rabi frequency of the repumping beam and, by varying this beam’s intensity, the ratio of coherent to incoherent pump rates could be varied. To wit, the effective decay rate of $|\uparrow\rangle$ was given by [199] $\Gamma = \Omega_p^2/\gamma$, where Ω_p was the Red Doppler (single-photon) Rabi frequency.⁹

In order to monitor the effects of the $T = 0$ reservoir on the motional *populations*, we created the state $|\psi\rangle = |\downarrow, 2\rangle$, then applied the $T = 0$ reservoir for a varying amount of time. Fig. 8.4 shows the motional level populations for $n = 0, 1, 2$ (as extracted from blue sideband flopping curves) after application of the $T = 0$ reservoir for various times t_{res} . As expected, the population in $|n = 2\rangle$ falls monotonically to zero. The population in $|n = 1\rangle$ initially grows from 0 as the $|n = 2\rangle$ population trickles down into it, but then it, too, is cleared out. Eventually, all the population ends up in $|n = 0\rangle$.

To determine the effects of the $T = 0$ reservoir upon the motional *coherences*, we produced the state $|\psi\rangle_i = |\downarrow\rangle(|0\rangle + |2\rangle)/\sqrt{2}$ in the manner described above (Sec. 8.2), then applied the $T = 0$ reservoir for a varying amount of time. We monitored the coherence (off-diagonal density matrix element) $\rho_{20} \equiv \rho_{\{\downarrow,2\}\{\downarrow,0\}}$. In order to determine the expected behaviour of this density matrix element, we may treat the simpler, two-level system originally proposed by Poyatos, Cirac, and Zoller [197]. However, in light

⁹ This formula holds when $\Omega_p \ll \gamma$.

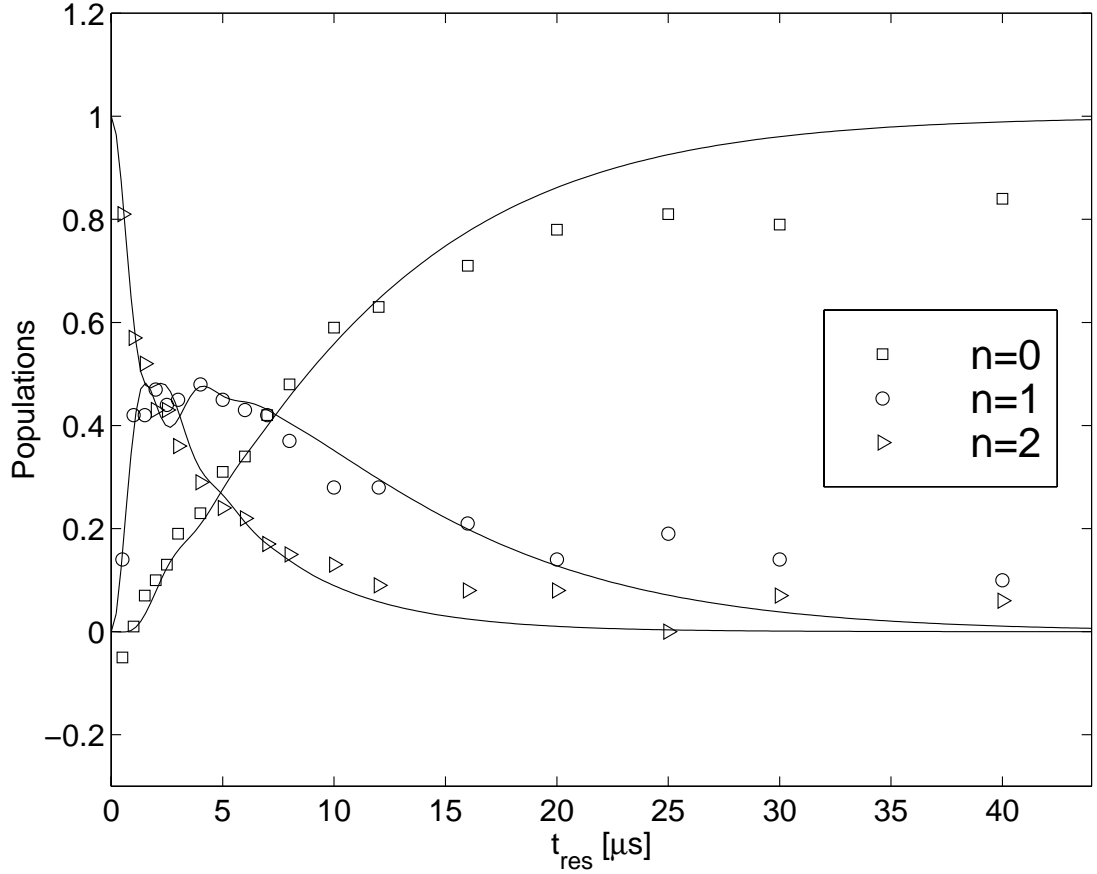


Figure 8.4: Populations of the motional levels $|0\rangle$, $|1\rangle$, and $|2\rangle$ as a function of the reservoir interaction time, for an initial $|\downarrow, 2\rangle$ state. The solid lines are fits to data of the master equation solutions.

of the above discussion, the incoherent pump rate, $\Gamma = \Omega_p^2/\gamma$, should be considered as a controllable parameter. The level scheme is sketched out in Fig. 8.5.

The correspondence between this level scheme and the $T = 0$ motional reservoir is worked out in Ref. [197]. However, in order to predict the results of the experiment, we may consider the master equation appropriate to the situation illustrated in Fig. 8.5(b). This master equation is:

$$\dot{\hat{\rho}} = i[\hat{\rho}, \hat{H}_S] + \frac{\Gamma}{2}(2\hat{\sigma}_- \hat{\rho} \hat{\sigma}_+ - \hat{\sigma}_+ \hat{\sigma}_- \hat{\rho} - \hat{\rho} \hat{\sigma}_- \hat{\sigma}_+), \quad (8.40)$$

where the red sideband coherent coupling Hamiltonian is given by

$$\hat{H}_S = g(\hat{a}^\dagger \hat{\sigma}_- + \hat{a} \hat{\sigma}_+), \quad (8.41)$$

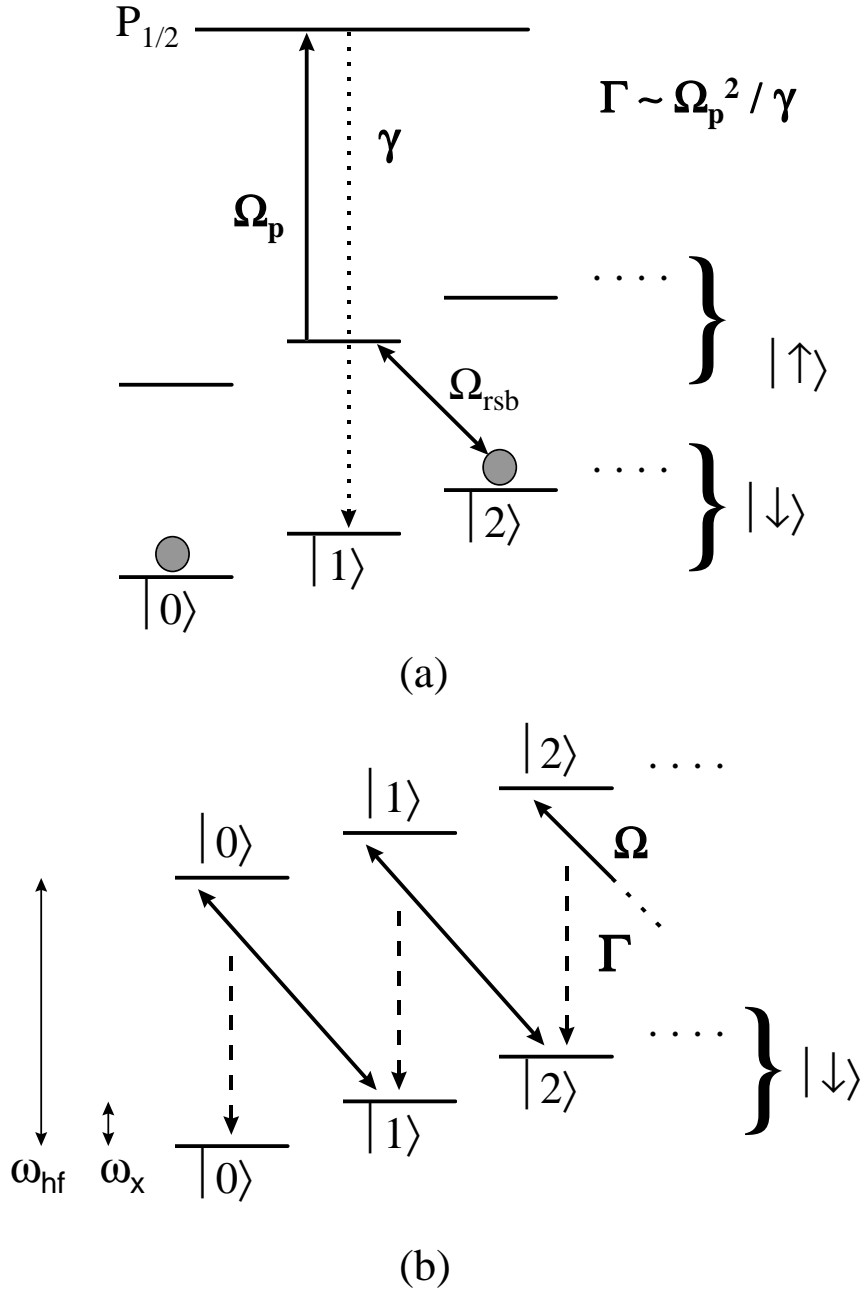


Figure 8.5: (a) Level scheme for realizing an engineered $T = 0$ amplitude reservoir. $|\downarrow, n\rangle$ and $|\uparrow, n-1\rangle$ are coupled on the red sideband, with Rabi frequency Ω_{rsb} . Repumping to $|\downarrow\rangle$ is accomplished by coupling $|\uparrow\rangle$ to the $2p \ ^2P_{1/2}$ level through a single-photon transition (Rabi frequency Ω_p) (driven by the “repumping” Red Doppler laser), from where it decays back to $|\downarrow\rangle$ at rate γ . The effective incoherent pump rate (for $\Omega_p \ll \gamma$) is $\Gamma = \Omega_p^2 / \gamma$. This scheme is essentially Raman cooling. (b) Effective two-level system equivalent to the scheme in (a). The coherent transfer rate is $\Omega = \Omega_{rsb}$ and the effective incoherent pump rate is $\Gamma = \Omega_p^2 / \gamma$.

where, from Eq. (3.7), $g = i\eta\hbar\Omega e^{i\phi}$. It is not hard to use Eq. 8.40 to find:

$$\dot{\rho}_{\{\downarrow 2\}\{\downarrow 0\}} = -i\sqrt{2}g\rho_{\{\uparrow 1\}\{\downarrow 0\}} \quad (8.42)$$

$$\dot{\rho}_{\{\uparrow 1\}\{\downarrow 0\}} = -i\sqrt{2}g\rho_{\{\downarrow 2\}\{\downarrow 0\}} - \frac{\Gamma}{2}\rho_{\{\uparrow 1\}\{\downarrow 0\}}. \quad (8.43)$$

The solution to this set of differential equations (given the initial state $|\psi\rangle_i$) is

$$\rho_{\{\uparrow 1\}\{\downarrow 0\}} = \frac{-i\sqrt{2}g}{2(\lambda_+ - \lambda_-)} \left[e^{\lambda_+ t} - e^{\lambda_- t} \right] \quad (8.44)$$

$$\rho_{\{\downarrow 2\}\{\downarrow 0\}} = \frac{1}{2(\lambda_+ - \lambda_-)} \left[\left(\lambda_+ + \frac{\Gamma}{2} \right) e^{\lambda_+ t} - \left(\lambda_- + \frac{\Gamma}{2} \right) e^{\lambda_- t} \right], \quad (8.45)$$

with

$$\lambda_{\pm} = -\frac{\Gamma}{4} \pm \frac{1}{2} \sqrt{\frac{\Gamma^2}{4} - 8g^2}. \quad (8.46)$$

Again, in the experiment, we monitor $\rho_{\{\downarrow 2\}\{\downarrow 0\}} \equiv \rho_{20}$.

Consider two limiting cases. In the first, $g \gg \Gamma$, so that the λ_{\pm} have an imaginary part. Here we expect an exponentially decaying cosine, which is precisely what we get:

$$\rho_{20} \rightarrow \frac{e^{-\Gamma/4t}}{2} \cos(\sqrt{2}gt). \quad (8.47)$$

In the limit $\Gamma \rightarrow 0$, the time dependence of ρ_{20} is sinusoidal. This reflects the fact that the red sideband drives Rabi oscillations between $|\downarrow, 2\rangle$ and $|\uparrow, 1\rangle$ which causes the density matrix element ρ_{20} to oscillate as the population in $|\downarrow, 2\rangle$ is driven out of that level.

In the second case $g \ll \Gamma$, so that λ_{\pm} is strictly real. In this case, it is easy to show that:

$$\rho_{20} \rightarrow \frac{1}{2}, \quad (8.48)$$

which is its initial value: the coherence never decays. This is an example of the quantum Zeno effect [59]. Before this regime is reached, the coherence exhibits exponential decay of the contrast with an extremely slow decay rate.

Figure 8.6 shows ρ_{20} (the Ramsey fringe contrast) as a function of t_{res} , for two different values of Ω_p . For small Ω_p , the Rabi flopping behaviour discussed above is

evident whereas, for larger incoherent pump rates (large Ω_p), the behaviour becomes more exponential in character. An interesting effect is that, for $\Gamma = \Omega_p^2/\gamma > \Omega_{rsb}$, the decay actually slows down with respect to the $\Gamma < \Omega_{rsb}$ case: this is an example of the quantum Zeno effect [59]. The initial slope of this curve is close to zero: this is an effect of non-exponential decay [200]. Another way to look at these effects is that, by changing the effective incoherent pump rate Γ , we were actually changing the effective bandwidth of the reservoir. In this sense, we were able to engineer the reservoir characteristics as desired.

8.5 Squeezed Reservoir

The Raman beams, in combination with an incoherent repumper, may also be used [197] to simulate a so-called “squeezed reservoir” interaction [124]:

$$\begin{aligned} \dot{\hat{\rho}}' = & \kappa \left[2(\mu\hat{a} + \nu\hat{a}^\dagger)\hat{\rho}'(\mu\hat{a} + \nu\hat{a}^\dagger)^\dagger \right. \\ & \left. - (\mu\hat{a} + \nu\hat{a}^\dagger)^\dagger(\mu\hat{a} + \nu\hat{a}^\dagger)\hat{\rho}' - \hat{\rho}'(\mu\hat{a} + \nu\hat{a}^\dagger)^\dagger(\mu\hat{a} + \nu\hat{a}^\dagger) \right], \end{aligned} \quad (8.49)$$

where $\mu^2 - \nu^2 = 1$. In order to realize such an interaction, the Raman beams must simultaneously be resonant with both the red and blue sidebands [197]. In this case, the ratio of the Rabi frequencies on the red and blue sidebands is given by μ/ν .

This interaction is actually quite analogous to the $T = 0$ reservoir: the only difference is that, in this case, the dark state of the interaction is a squeezed state, rather than the $|n = 0\rangle$ Fock/coherent state. In both cases, the entropy of the ion’s motional state is reduced, and changes from that of a mixed state to that of a pure state. The only difference is the particular pure state to which the ion relaxes (i.e. the dark state of the interaction).

We illuminated the ion simultaneously with the red and blue sidebands by replacing the usual Red Raman switch AOM by two AOMs (one whose drive rf was at frequency $80 \text{ MHz} - \omega_z$ and the other’s at $80 \text{ MHz} + \omega_z$), then combining the two beams

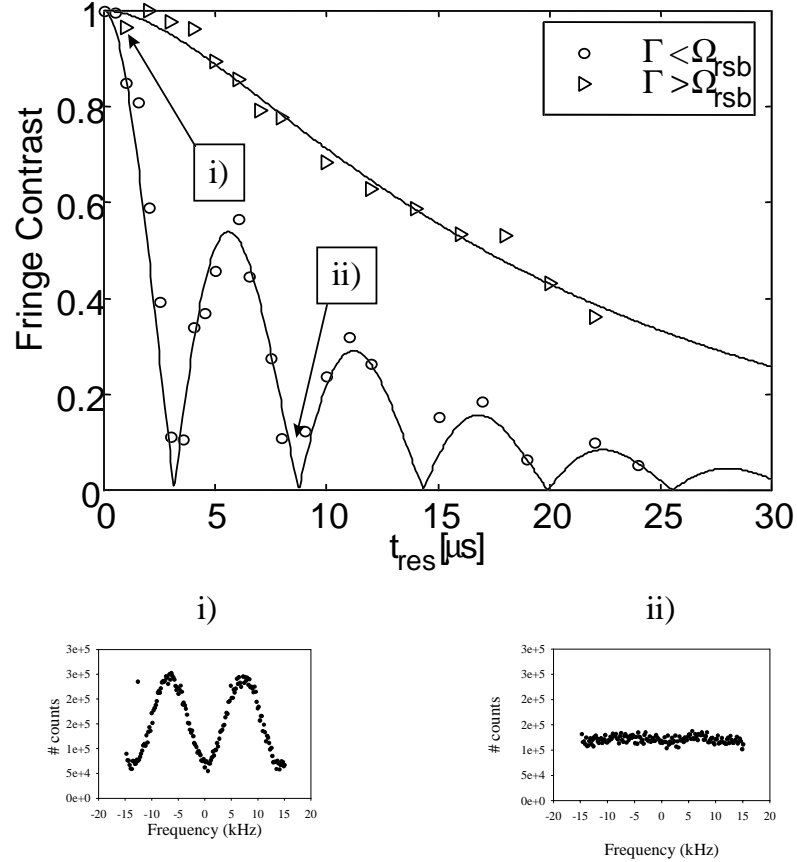


Figure 8.6: Evolution of the coherence ρ_{02} for an initial $|\downarrow\rangle(|0\rangle + |2\rangle)/2^{1/2}$ state, as a function of the interaction time t_{res} with an engineered $T = 0$ reservoir. Two cases are shown, indicating the two regimes of behaviour: one where the incoherent pump rate is greater than the coherent rate, and one where the opposite is true. Notice that, for the case $\Gamma > \Omega_{rsb}$, the decay is actually slower. This is consistent with the predicted dynamics (Eq. (8.45)), and represents a Zeno effect. The low slope near $t_{res} = 0$ indicates non-exponential decay.

on a beamsplitter before the input lens to the trap. However, since the underlying process behind the squeezed reservoir interaction is a squeezing process, the interaction is of order η^2 , and thus slow. At the time we tried the experiments, the heating rate in the trap overwhelmed the “cooling” rate of the squeezed reservoir interaction, preventing us from observing the effects of the reservoir.